molbank

MDPI

Communication

Phosphine–Stibine and Phosphine–Stiborane *peri*-Substituted Donor–Acceptor Complexes

Jan U. Bergsch, Alexandra M. Z. Slawin, Petr Kilian and Brian A. Chalmers *

EaStCHEM School of Chemistry, University of St Andrews, North Haugh, St Andrews, Fife KY16 9ST, UK
* Correspondence: bac8@st-andrews.ac.uk; Tel.: +44-1334-463-785

Abstract: Two novel Sb(III) and Sb(V) *peri*-substituted acenaphthene phosphorus−antimony compounds were prepared. The Sb(III) compound, **1**, was prepared via reacting the organolithium precursor with dichloro(*p*-tolyl)Stibine, and **2** was prepared by the chlorination of **1**. Both **1** and **2** were characterized by multinuclear (^{1}H, ^{13}C and ^{31}P) NMR spectroscopy, and their molecular structures resolved by single-crystal X-ray diffraction. Both compounds show a dative P−Sb interaction with the antimony being the acceptor group in both cases owing to its Lewis acidity.

Keywords: X-ray crystallography; donor–acceptor; p-block chemistry; NMR spectroscopy; inert atmosphere synthesis; phosphorus; antimony

1. Introduction

A comprehensive series of phosphine–stibine and phosphine–stiborane donor–acceptor complexes supported by *peri*-substituted acenaphthyl scaffolds was reported, to study the onset of the P→Sb donor–acceptor interaction [1]. The diisopropylphosphino (−P*i*Pr$_2$) donor group was maintained throughout the series, with the acceptor groups including all pentavalent permutations of −SbCl$_n$Ph$_{4-n}$ (n = 0–4) and trivalent groups −SbCl$_n$Ph$_{2-n}$ (n = 0–2) (Figure 1). Compounds with similar structural features, such as diphenylphosphino donor groups, have also been reported [2–4]. By altering the Lewis acidity of the acceptor group, the P→Sb dative interaction ranged from strongly bonding, to non-bonding, with the P−Sb distances ranging from 2.5923(17) Å in **A** to 3.1247(16) Å in **H**, as indicated by their calculated Wiberg Bond Index (WBI) [1,5].

The Sb(III) compounds, **A**–**C**, each display a slightly different structure. In **A**, there is a clearly bonding P−Sb interaction (2.5923(17) Å), which elongates slightly to 2.7104(8) or 2.7244(9) Å when one chlorine is swapped for a phenyl or mesityl group in $\mathbf{B_{Ph}}$ and $\mathbf{B_{Mes}}$. The 'normal' range for a λ^3P−λ^3Sb bond is (2.49–2.59Å) [6]. However, the lack of in-plane and out-of-plane distortions in the acenaphthene ring system indicates a P−Sb bond in $\mathbf{B_{Ph}}$ and $\mathbf{B_{Mes}}$. In both $\mathbf{B_{Ph}}$ and $\mathbf{B_{Mes}}$, the aryl group and chlorine are adjacent to one another (Cl−Sb−C$_{Ph}$ 88.49(7)° and Cl−Sb−C$_{Mes}$ 87.00(6)°), but there is a quasi-linear P−Sb−Cl interaction with a 170.34(5)° and 168.07(2)° angle, respectively. The major difference between $\mathbf{B_{Ph}}$ and $\mathbf{B_{Mes}}$ is that the mesityl ring shows restricted rotation in solution due to the *ortho* methyl groups causing a steric clash with the acenaphthene and adjacent isopropyl groups. This is apparent in the ^{1}H NMR spectrum as there are three separate methyl signals for the mesityl group at δ_H 2.83, 2.20, and 1.90 ppm. In **C**, the P···Sb distance increases to 3.191(1) Å and shows a significant drop in WBI to 0.15 vs. 0.74 and 0.48 for **A** and $\mathbf{B_{Ph}}$/$\mathbf{B_{Mes}}$, respectively. Whilst this distance is still sub-van der Waals (Σr_{vdW} (P, Sb) = 4.15 Å), the evidence points at a lack of direct P−Sb bond, likely due to the weakly Lewis-acidic −SbPh$_2$ acceptor group [7].

Herein, we report the synthesis and full characterization of compounds **1** and **2**, which are analogues of $\mathbf{B_{Ph}}$, $\mathbf{B_{Mes}}$, and **E**, with *para*-tolyl groups instead of phenyl groups. The *p*-tolyl derivatives were selected as these were expected to decrease the electrophilicity of

check for updates

Citation: Bergsch, J.U.; Slawin, A.M.Z.; Kilian, P.; Chalmers, B.A. Phosphine–Stibine and Phosphine–Stiborane *peri*-Substituted Donor–Acceptor Complexes. *Molbank* **2023**, *2023*, M1653. https://doi.org/10.3390/M1653

Received: 5 May 2023
Revised: 22 May 2023
Accepted: 24 May 2023
Published: 30 May 2023

the Sb groups slightly compared to the phenyl-substituted compounds. This fine-tuning was hoped to provide additional insight into the sudden structural changes observed on transition from $\mathbf{B_{Ph}}$/$\mathbf{B_{Mes}}$ to **C**.

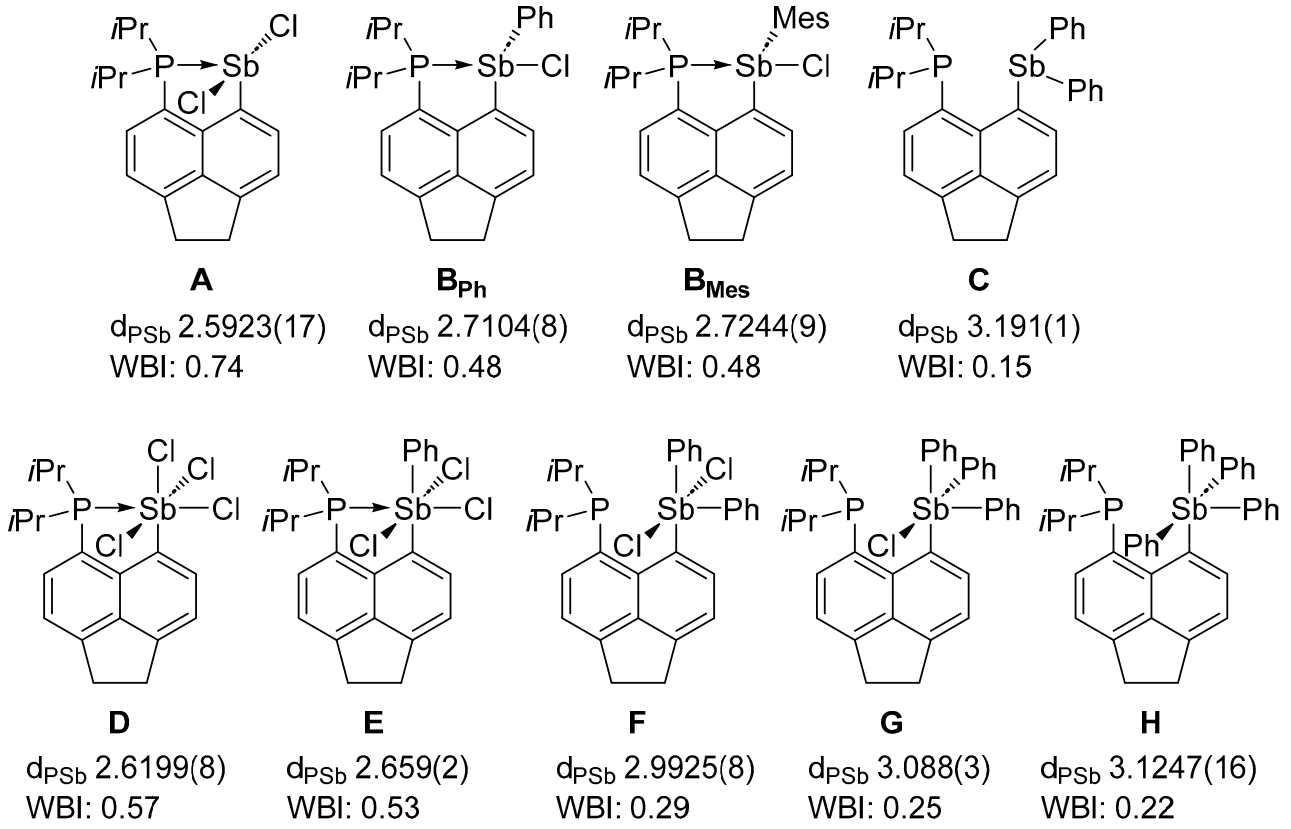

Figure 1. Series of phosphorus–antimony *peri*-substituted compounds with $d_{P...Sb}$ (Å) and WBI shown.

2. Results and Discussion

2.1. Synthesis and Spectroscopy

Due to the scarce commercial availability of organostibine compounds, *p*-tolSbCl$_2$ was prepared in two steps. Firstly, (*p*-tol)$_3$Sb was prepared from SbCl$_3$ and *p*-tolylmagnesium bromide to afford crystalline (*p*-tol)$_3$Sb in 79% yield (Scheme 1). It is well established that organohalostibines can be prepared by melting R$_3$Sb and SbX$_3$ together in the appropriate stoichiometric ratio [8]. Thus, freshly prepared (*p*-tol)$_3$Sb was combined with SbCl$_3$ in a 1:2 ratio, affording pure *p*-tolSbCl$_2$ after recrystallisation.

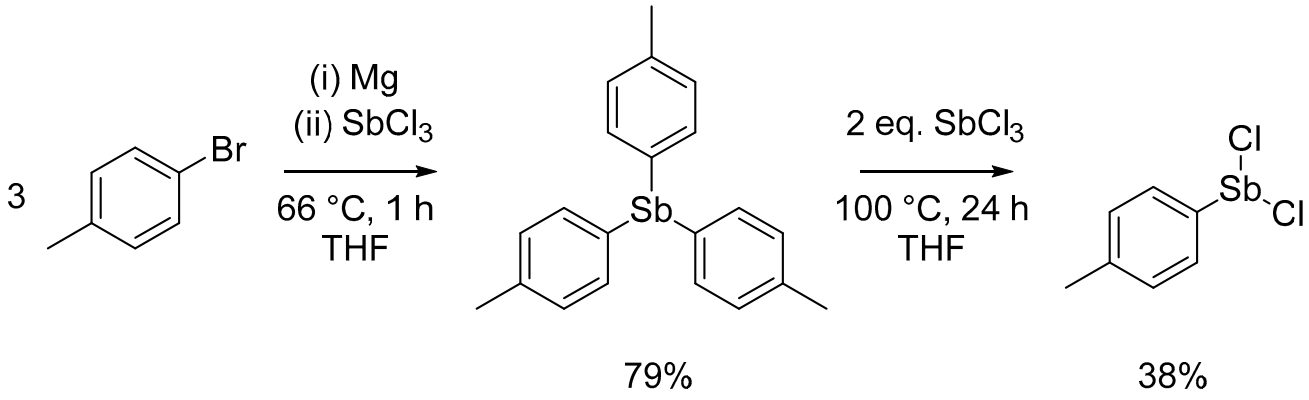

Scheme 1. The synthesis of *p*-tolSbCl$_2$ from the (*p*-tol)$_3$Sb and SbCl$_3$ with isolated yields.

The other precursor, 5-bromo-6-(diisopropylphosphino)acenaphthene (**P**), was prepared according to the literature procedure by the reaction of 5,6-dibromoacenaphthene with *n*-butyllithium followed by chlorodiisopropylphosphine [9,10]. **P** was subsequently reacted with an equivalent of *n*-butyllithium. Following, a solution of dichloro(*p*-tolyl)stibine in diethyl ether was added slowly over an hour to avoid multiple substitution. After filtration to remove the insoluble lithium salts and washing with degassed distilled water, **1** was obtained as a white powder, in a 74% yield (Scheme 2). Compound **1** was found to be stable with respect to water, but sensitive to oxygen, thus was stored in an argon atmosphere glovebox.

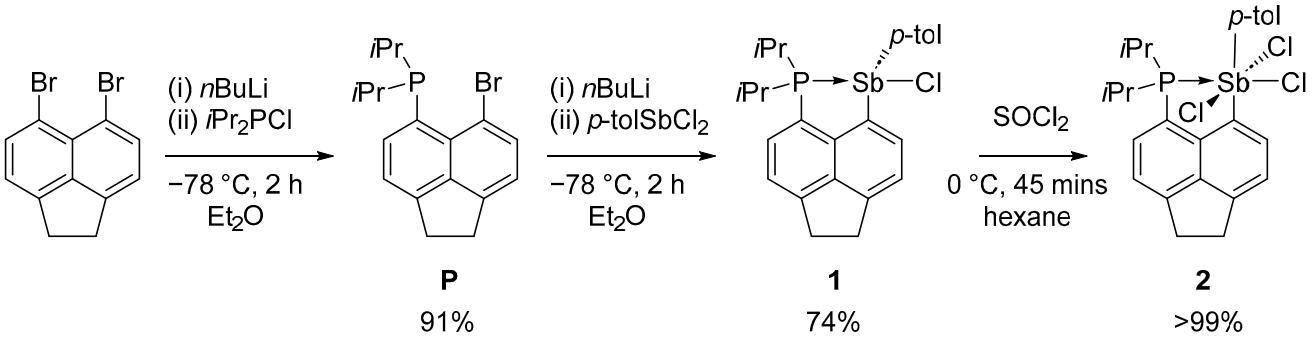

P 91%

1 74%

2 >99%

Scheme 2. Preparation of Compounds **1** and **2** with isolated yields.

In **A**–**C**, the phosphorus atom becomes increasingly deshielded over the series (**A**–**C**, δ_P 51.0, 1.5, and −21.9 ppm, respectively) as the Lewis acidity of the Sb acceptor group decreases. The $^{31}P\{^1H\}$ NMR spectrum of **1** shows a sharp singlet at δ_P 1.2 ppm. This is a very subtle change in δ_P when compared to **P** (δ_P −2.2 ppm). This is also very similar to the chemical shift observed for $\mathbf{B_{Ph}}$ and $\mathbf{B_{Mes}}$ (δ_P 1.5 and −3.6 ppm, respectively). The isopropyl groups are magnetically inequivalent, as seen in the ^1H NMR spectrum. Each methyl group shows a doublet of doublets with $^3J_{HP}$ and $^3J_{HH}$ coupling (ranging 7–18 Hz) at δ_H 1.19, 1.09, 0.79, and 0.45 ppm. The fact that all four methyl groups of the *i*Pr$_2$P− moiety are in different magnetic environments provides additional evidence of a direct P−Sb bond, resulting in restricted rotation around the P−C_{Acenap} and Sb−C_{Acenap} bonds, "locking" the *para*-tolyl group and the isopropyl groups. High Resolution Mass Spectrometry (HRMS) confirmed the presence of the *para*-tolyl group, as the M−Cl ion was observed as the base peak. The pattern also follows the predicted isotopic distribution owing to the natural abundance of ^{121}Sb and ^{123}Sb.

The antimony(V) compound, **2**, was prepared by chlorination of **1** using sulfuryl chloride akin to the method used to prepare **E** from $\mathbf{B_{Ph}}$ [1]. Compound **2** was obtained as a pale-yellow powder in a quantitative yield. The $^{31}P\{^1H\}$ NMR spectrum of **2** shows a sharp singlet at δ_P −30.2 ppm, showing a significant shielding of the phosphorus nucleus, due to the very Lewis-acidic -SbCl$_3$R group. This is a very subtle change in δ_P when compared to **E** (*c.f.* δ_P −28.4 ppm). The HRMS was able to confirm that the chlorination had taken place with the M−Cl being observed as base peak. As above, the pattern also follows the predicted isotopic distribution owing to the natural abundance of ^{121}Sb and ^{123}Sb, as well as ^{35}Cl and ^{37}Cl.

Contrarily to **1**, the ^1H NMR spectrum of **2** shows only two separate doublets of doublets for the methyl groups within the isopropyl groups at δ_H 1.34 and 1.20 ppm, suggesting that **2** has a plane of symmetry in the molecule along the P−Sb axis. This suggests that the phosphine group, acenaphthene and *p*-tolyl groups adopt a *mer* arrangement to one another, leaving the three chlorine atoms in a *mer* arrangement around antimony in its pseudo-octahedral coordination environment.

2.2. X-ray Crystallography

Crystals of **1** suitable for single-crystal X-ray diffraction were grown from acetonitrile at ambient conditions. The structure of **1** is shown in Figure 2, and selected parameters are listed in Table 1. There is a dative bonding interaction between the phosphorus and antimony, with a bond length of 2.7422(7) Å. This is marginally longer than that in $\mathbf{B_{Ph}}$ (2.7104(8) Å), indicating a subtly weaker interaction due to the *p*-tolyl group being slightly more electron-donating than the phenyl group. A marginal shortening of the Sb−Cl bond from 2.6798(7) Å in $\mathbf{B_{Ph}}$ to 2.6678(7) Å in **1** also takes place. There are no significant distortions in the acenaphthene ring system with the P and Sb atoms displaced by only 0.164 and 0.053 Å, respectively, from the mean C_{12} plane. There is a very small P9−C9···C1−Sb1 dihedral angle of 2.7(1)°, indicating a bonding interaction between the phosphine and stibine groups.

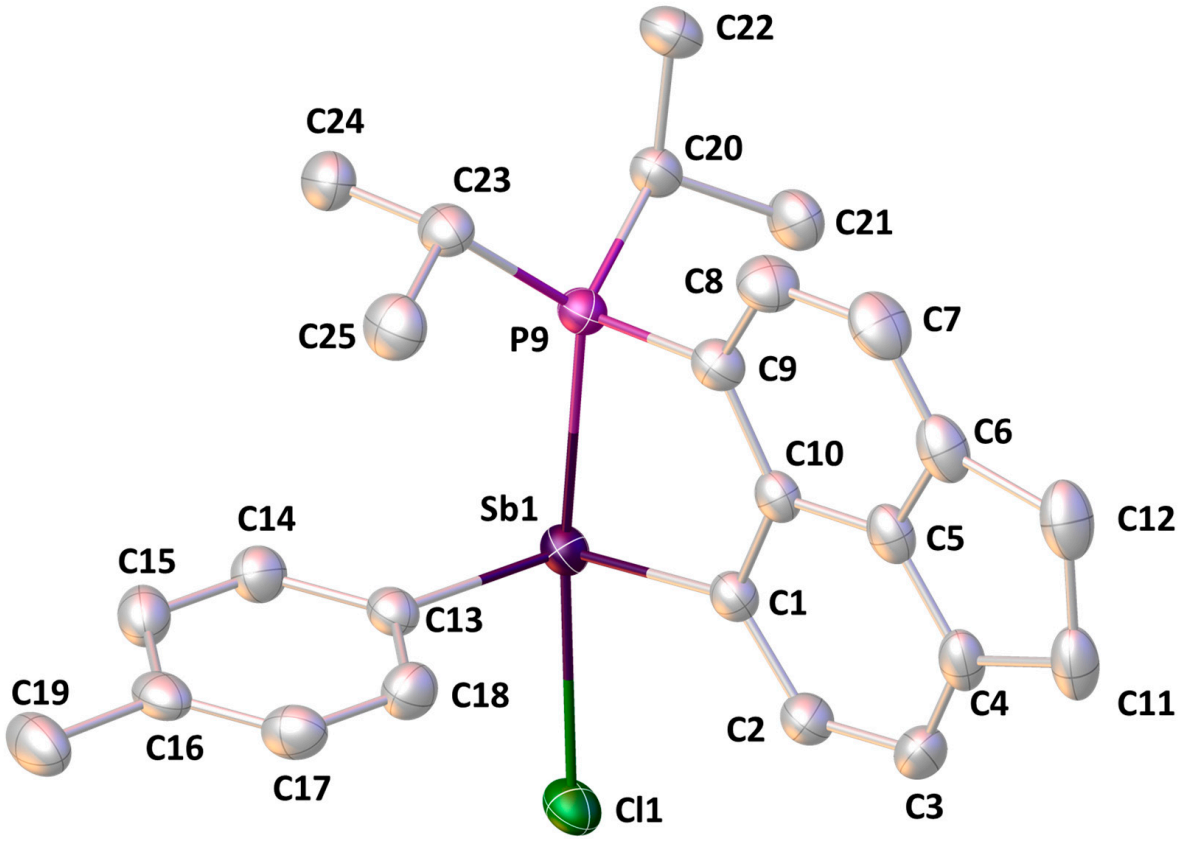

Figure 2. Molecular structure of **1**. Hydrogen atoms are omitted for clarity. Anisotropic displacement ellipsoids are set at the 50% probability level.

Table 1. Selected bond lengths (Å), angles (°), and dihedral angles (°) for **1** and **2**.

	1	**2**
P9−Sb1	2.7422(7)	2.7086(6)
Sb1−Cl	2.6674(7)	2.4476(5)−2.4836(7)
P9−C	1.798(3)−1.854(3)	1.806(2)−1.846(2)
Sb1−C	2.144(2)−2.172(2)	2.138(2), 2.152(2)
C9−P9−Sb1	97.97(8)	95.20(6)
P9−Sb1−Cl_{trans}	167.83(2)	171.52(2)
P9−Sb1−Cl_{cis}	–	83.88(2), 94.69(2)
Cl−Sb1−Cl	–	90.01(2), 90.92(2)
P9−Sb1−C_{Ph}	88.49(6)	97.50(5)
P9−C9···C1−Sb1	2.7(1)	3.71(8)
Splay angle †	3.9(6)	3.4(4)

† Splay angle = (Sb1−C1−C10) + (C1−C10−C9) + (C10−C9−P9) − 360.

The mesityl analogue $\mathbf{B_{Mes}}$ shows many of the same features as **1** with very similar P−Sb and Sb−Cl bond lengths (2.7244(9) and 2.6682(9) Å, respectively). Compound **1** represents the intermediate between $\mathbf{B_{Ph}}$ and $\mathbf{B_{Mes}}$ in terms of the Lewis acidity of the stibine group. However, the differences between all three structures are very subtle. The P−Sb bond length shows a marginal increase from $\mathbf{B_{Ph}}$ to **1**, which is reflected in the decrease in δ_P as the phosphorus becomes slightly more shielded. However, from **1** to $\mathbf{B_{Mes}}$, the δ_P decreases again, but the P−Sb bond shortens slightly. This is attributed to the increased steric bulk of the mesityl group versus the phenyl or *para*-tolyl group.

The antimony atom adopts a distorted pseudo-trigonal bipyramidal geometry with the axial positions taken up by the chlorine and phosphorus atoms, with a P9−Sb1−Cl1 angle of 167.83(2)°. The C1, C13 atoms, and lone pair adopt the equatorial positions with P9−Sb1−C13 of 88.61(5)° (Table 1). The proximity of one of the isopropyl groups to the π-cloud of the *p*-tolyl ring is evident. This results in CH···π interactions of 2.761 Å between H25B···Cg(C13–C18) (See Supplementary Materials, Figure S1). The Sb1−Cl1 bond length is 2.6674(7) Å, which is longer than that in $SbCl_3$ (cf. 2.360 Å); however, it is comparable to that found in **B** (2.6798(8) Å). The lengthening of this bond is associated with the donation of the phosphine lone-pair electron density into the σ*(Sb−Cl) orbital. The phosphorus atom adopts a distorted tetrahedral geometry, with distortions arising due to the rigid acenaphthene backbone enforcing the C9−P9−Sb1 angle of 97.97(8)°.

Crystals of **2** suitable for single-crystal X-ray diffraction were grown from acetonitrile at ambient conditions. The X-ray structure confirmed that the structure postulated via the ^{1}H and ^{31}P NMR spectra (Figure 3). There is a dative interaction between the phosphorus and antimony atoms, with a bond length of 2.7086(6) Å. This is marginally shorter than **1,** indicating a subtly stronger interaction due to increased Lewis acidity of the antimony acceptor group, stemming from the addition of two chlorine atoms. The *p*-tolyl group is slightly more electron-donating than the phenyl group; thus, the P−Sb bond length is increased slightly when compared to **E** (2.659(2) Å) as the -$SbCl_3$Ph group is slightly more Lewis-acidic than the -$SbCl_3$(*p*-tol) group. There are no significant distortions in the acenaphthene ring system with the P and Sb atoms displaced by only 0.016 and 0.105 Å, respectively, from the mean C_{12} plane. There is a very small P9−C9···C1−Sb1 dihedral angle of 3.71(8)°, indicating a bonding interaction between the phosphine and stibine groups.

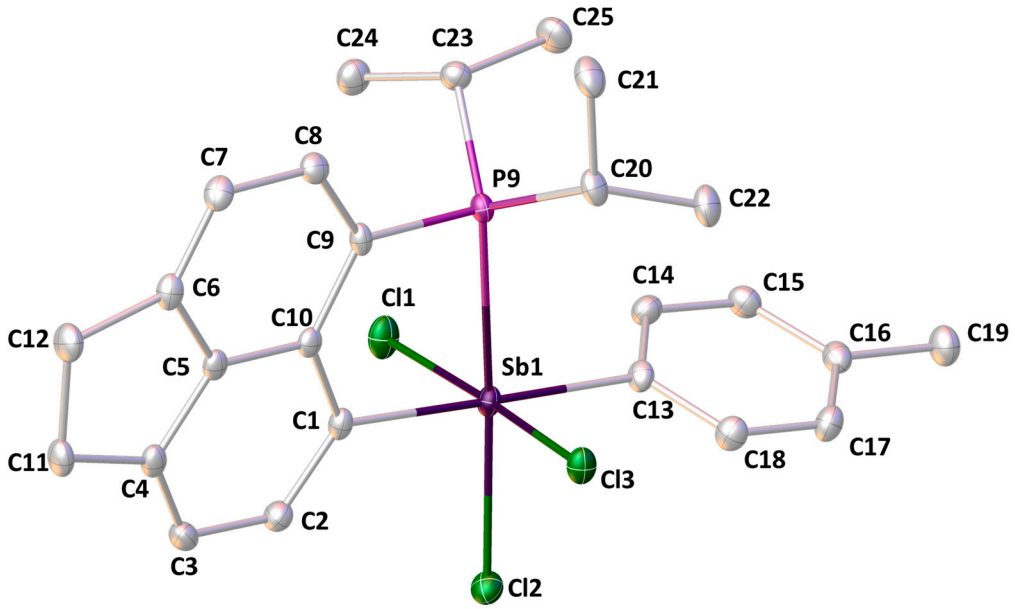

Figure 3. Molecular structure of **2**. Hydrogen atoms are omitted for clarity. Anisotropic displacement ellipsoids are set at the 50% probability level.

The phenyl analogue, **E**, shows many of the same features as **2** with very similar Sb−Cl bond lengths (ranging 2.449(2)–2.469(2) in **E**, *c.f.* 2.4476(5)–2.4836(7) Å in **2**) and angles. The antimony atom attains octahedral geometry with acenaphthene and *p*-tolyl groups being *trans* (C1−Sb1−C13 178.25(7)°) and the three chlorine atoms adopting the *mer* geometry with *cis*-angles P−Sb−Cl ranging 83.88(2)–94.69(2)° and *cis*-angles Cl−Sb−Cl ranging 90.01(2)–90.92(2)° (Table 1). The Sb−Cl bond lengths are all much shorter in **2** than **1**, (ranging 2.4476(5)–2.4836(7) Å in 2, *c.f.* 2.6674(7) Å in **1**). These are longer than those found in $SbCl_3$ (2.360 Å); however, those in **2** are comparable to those found in **E** (2.449(2)–2.469(2) Å). Similarly to **1**, the phosphorus atom in **2** adopts a distorted tetrahedral geometry with the most acute angle being C9−P9−Sb1 (95.20(6)°).

3. Materials and Methods

3.1. General Considerations

All synthetic manipulations were performed under an atmosphere of dry nitrogen using standard Schlenk Techniques or under an argon atmosphere in a Saffron glove box. All glass apparatus was stored in a drying oven (*ca*. 120 °C) prior to use. Dry solvents were collected from an MBraun Solvent Purification System and stored over appropriate molecular sieves. Water used in experiments was subjected to nitrogen sparging and stored under nitrogen prior to use. Chemicals were taken from the laboratory inventory and used without further purification with the exception of antimony(III) chloride, which was sublimed in vacuo and stored under argon prior to use.

All NMR spectra were recorded using a JEOL GSX Delta (270 MHz) or Bruker Avance III (500 MHz) spectrometer at 25 °C. Assignments of ^{1}H and ^{13}C spectra were made in conjunction with the appropriate 2D spectra. ^{13}C NMR spectra were recorded using the DEPTQ pulse sequence with broadband proton decoupling. For ^{1}H and ^{13}C NMR, tetramethylsilane was used as an external standard. For ^{31}P NMR, 85% H_3PO_4 in D_2O was used as the external standard. Residual solvent peaks were also used for secondary calibration ($CDCl_3$ δ_H 7.260 ppm; δ_C 77.160 ppm). Chemical shifts (δ) are given in parts per million (ppm). Coupling constants (*J*) are quoted in Hertz (Hz).

Melting and decomposition points were determined by heating solid samples in sealed glass capillaries using a Stuart SMP30 Melting Point Apparatus (Cole-Parmer, Cambridge, UK). Mass Spectrometry was performed at the EPSRC UK National Mass Spectrometry Facility in Swansea using a Thermofisher LTQ Orbitrap XL. Elemental Analysis was performed by the EA Service at London Metropolitan University (London, UK).

3.2. Synthetic Procedures

3.2.1. Synthesis of Tris(*p*-tolyl)Stibine

A solution of *p*-bromotoluene (21.6 mL, 30.00 g, 175 mmol) in dry tetrahydrofuran (200 mL) was slowly added to pre-dried magnesium turnings (4.26 g, 175 mmol) until the Grignard reaction had initiated. After this, the remaining mixture was added dropwise to the magnesium over one hour. After addition, the solution was heated under reflux for one hour. Upon cooling to ambient conditions, a solution of antimony(III) chloride (13.54 g, 58.33 mmol) in diethyl ether (75 mL) was added dropwise over one hour. After addition, the solution was brought to reflux for a further hour. Upon cooling to ambient conditions, water (50 mL) was added cautiously to the mixture. The organic layer was separated and dried over sodium sulfate. The volatiles were removed in vacuo to afford a pale-yellow solid, which was washed with ethanol (5 × 5 mL) and dried in vacuo to yield the desired material as a white solid (18.12 g, 79%) (M.p. 126 °C). **^{1}H NMR** (270.0 MHz, $CDCl_3$) δ_H 7.33 (6H, d, $^{3}J_{HH}$ 7.9 Hz, *o*-H), 7.13 (6H, d, $^{3}J_{HH}$ 7.9 Hz, *m*-H), 2.34 (9H, s, CH_3); **^{13}C DEPTQ NMR** (100.6 MHz, $CDCl_3$) δ_C 138.3 (s, qC_{ipso}), 136.2 (s, *o*-CH), 134.8 (s, q<u>C</u>Me), 129.7 (s, *m*-CH), 21.4 (s, CH_3).

3.2.2. Synthesis of Dichloro(*p*-tolyl)Stibine

This procedure was inspired from the literature synthesis of $PhSbCl_2$ [1,8]. Solid tris(*p*-tolyl)stibine (14.70 g, 45.9 mmol) and solid antimony(III) chloride (19.10 g, 103.2 mmol) were combined and heated to 100 °C for 24 h, forming a viscous pale-yellow melt. This was cooled to ambient conditions, where it solidified. The solid was extracted with boiling pentane: chloroform (1:1 *v*/*v*) (2 × 25 mL) and immediately filtered. The combined fractions were concentrated to $\frac{1}{4}$ of the initial volume and cooled to −20 °C. Colourless crystals of the desired product were isolated via filtration and dried in vacuo and stored under argon until required (14.69 g, 38%) (M.p. 91 °C). **^{1}H NMR** (270.0 MHz, $CDCl_3$) δ_H 7.75 (2H, d, $^3J_{HH}$ 8.0 Hz, *o*-H), 7.38 (2H, d, $^3J_{HH}$ 8.0 Hz, *m*-H), 2.40 (3H, s, CH_3); **^{13}C DEPTQ NMR** (100.6 MHz, $CDCl_3$) δ_C 148.6 (s, qC_{ipso}), 142.3 (s, q<u>C</u>Me), 132.8 (s, *o*-CH), 130.4 (s, *m*-CH), 21.7 (s, CH_3).

3.2.3. Synthesis of **1**

To a cooled (−78 °C), rapidly stirring solution of **P** (1.00 g, 2.86 mmol) in diethyl ether (25 mL), a solution of *n*-butyllithium in hexane (1.15 mL, 2.5 M, 2.86 mmol) was added over one hour. The mixture was maintained stirring at −78 °C for a further two hours. Following this, a solution of dichloro(*p*-tolyl)stibine (0.81 g, 2.86 mmol) in diethyl ether (15 mL) was added over 15 min whilst maintaining −78 °C. After addition, the reaction mixture was warmed to ambient conditions overnight. The solid that formed was collected via filtration and rapidly washed with water to afford a colourless powder (1.10 g, 74%) (Mp. 223 °C with decomposition). Crystals suitable for X-ray diffraction were grown from acetonitrile at ambient conditions. The NMR numbering scheme is provided in Figure 4. **Elemental Analysis**: Calcd. (%) for $C_{25}H_{29}PSbCl$: C 58.00, H 5.65; found C 57.91 H 5.58; **^{1}H NMR** (500.1 MHz, $CDCl_3$) δ_H 9.14 (1H, d, $^3J_{HH}$ 7.2 Hz, H-8), 7.61 (1H, d, $^3J_{HH}$ 7.2 Hz, H-7), 7.57 (1H, dd~t, $^3J_{HP}$ 7.1, $^3J_{HH}$ 7.0 Hz, H-2), 7.37 (1H, d, $^3J_{HH}$ 7.0 Hz, H-3), 7.34 (2H, d, $^3J_{HH}$ 7.5 Hz, H-17), 6.99 (2H, d, $^3J_{HH}$ 7.5 Hz, H-18), 3.54−3.44 (4H, m, H-11,12), 2.43 (1H, h, $^3J_{HH}$ 7.3 Hz, H-13/13′), 2.37−2.26 (1H, m, H-13/13′), 2.23 (3H, s, H-20), 1.23−1.16 (3H, m, H-14/14′), 1.09 (3H, dd, $^3J_{HP}$ 17.3, $^3J_{HH}$ 7.0 Hz, H-14/14′), 0.79 (3H, dd, $^3J_{HP}$ 17.3, $^3J_{HH}$ 7.0 Hz, H15/15′), 0.45 (3H, dd, $^3J_{HP}$ 15.0, $^3J_{HH}$ 7.1 Hz, H-15/15′); **^{13}C DEPTQ NMR** (125.8 MHz, $CDCl_3$) δ_C 152.1 (s, qC-4), 148.0 (s, qC-6), 144.4 (d, $^2J_{CP}$ 28.9 Hz, qC-10), 140.6 (d, $^4J_{CP}$ 4.1 Hz, C-8), 140.5 (s, qC-5), 138.6 (s, qC-19), 136.3 (s, qC-16), 135.5 (s, C-17), 135.4 (s, qC-9), 133.4 (d, $^2J_{CP}$ 3.2 Hz, C-2), 129.9 (s, C-18), 122.8 (d, $^1J_{CP}$ 21.0 Hz, qC-1), 122.2 (s, C-7), 119.6 (d, $^3J_{CP}$ 13.9 Hz, C-3), 31.0 (s, C-11/12), 30.3 (s, C-11/12), 24.9 (d, $^1J_{CP}$ 4.7 Hz, C-13/13′), 24.4 (d, $^1J_{CP}$ 14.1 Hz, C-13/13′), 21.5 (s, C-20), 19.2 (s, C-14/14′), 19.2 (s, C14/14′), 18.1 (s, C-15/15′), 17.3 (s, C-15/15′); **^{31}P{^{1}H} NMR** (202.5 MHz, $CDCl_3$) δ_P 1.2 (s); **HRMS** (ES+): *m*/*z* calcd. for $C_{25}H_{29}PSb$: 481.1045, found 481.1029 [M − Cl].

3.2.4. Synthesis of **2**

To a cooled (0 °C) rapidly stirring suspension of 1 (500 mg, 969 µmol), in *n*-hexane (20 mL), a solution of sulfuryl chloride (94 µL, 1.17 mmol) in *n*-hexane (6 mL) was added dropwise over 15 min. The solution was maintained stirring at 0 °C for a further 30 min. The volatiles were removed in vacuo affording a yellow powder in a quantitative yield (570 mg) (M.p. 227 °C with decomposition). Crystals suitable for X-ray diffraction were grown from acetonitrile at ambient conditions. The NMR numbering scheme is provided in Figure 4. **^{1}H NMR** (500.1 MHz, $CDCl_3$) δ_H 8.88 (1H, dd, $^3J_{HH}$ 7.5, $^4J_{HP}$ 2.4 Hz, H-8), 8.50 (2H, dd, $^3J_{HH}$ 8.4, $^4J_{HP}$ 1.9 Hz, H-17), 7.78 (1H, dd~t, $^3J_{HH}$~$^3J_{HP}$ 7.3 Hz, H-2), 7.54 (1H, dd, $^3J_{HH}$, $^5J_{HP}$ 1.4 Hz, H-7), 7.47 (1H, d, $^3J_{HH}$ 7.4 Hz, H-3), 7.33 (2H, $^3J_{HH}$ 8.4 Hz, H-18), 3.53−3.44 (4H, m, H-11,12), 3.00−2.90 (2H, m, H-13,13′), 2.42 (3H, s, H-20), 1.31 (6H, dd, $^3J_{HP}$ 15.9, $^3J_{HH}$ 7.1 Hz, H-14,14′), 1.18 (6H, dd, $^3J_{HP}$ 16.9, $^3J_{HH}$ 7.3 Hz, H-15,15′). **^{13}C DEPTQ NMR** (125.8 MHz, $CDCl_3$) δ_C 159.8 (d, $^2J_{CP}$ 52.6 Hz, qC-16), 153.5 (s, qC-6), 152.9 (s, qC-4), 149.2 (s, qC-9), 140.8 (s, qC-19), 139.8 (d, $^3J_{CP}$ 7.1 Hz, qC-5), 134.0 (s, C-2), 130.7 (s, qC-10), 129.9 (s, C-17), 129.7 (s, C-18), 129.3 (d, $^3J_{CP}$ 8.0 Hz, C-8), 121.2 (d, $^5J_{CP}$ 5.9 Hz, C-7), 119.7 (d, $^3J_{CP}$ 6.8 Hz, C-3), 115.3 (d, $^1J_{CP}$ 36.8 Hz, qC-1), 31.2 (s, C-11/12), 30.1 (s, C-11/12),

26.5 (d, $^{1}J_{CP}$ 14.5 Hz, C-13,13′), 21.3 (s, C-20), 19.5 (s, C-15,15′), 18.9 (s, C-114,14′); **^{31}P{^{1}H} NMR** (202.5 MHz, $CDCl_3$) δ_P −30.2 (s); HRMS (ES+): *m*/*z* calcd. for $C_{25}H_{29}PSbCl_2$ 551.0422, found 551.0417 [M − Cl].

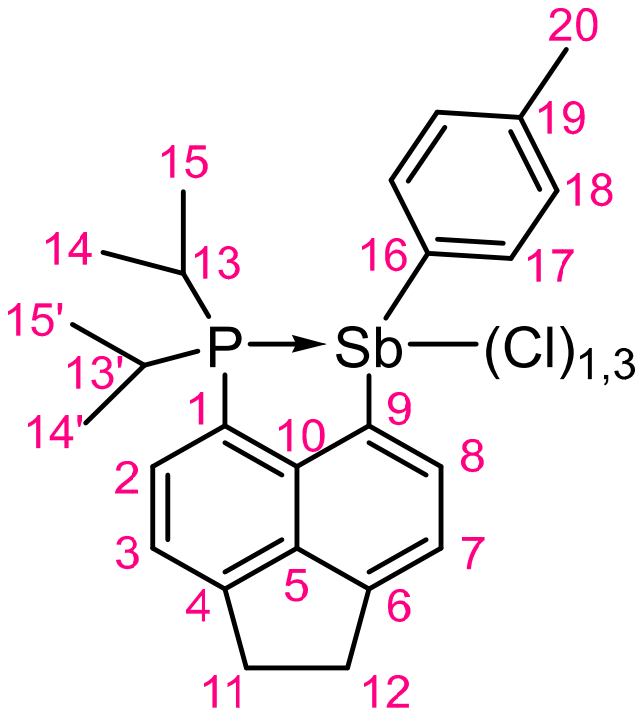

Figure 4. NMR Numbering Scheme for **1** and **2**.

3.2.5. Crystallographic Details

Colourless crystals of **1** and **2** were independently grown from acetonitrile at ambient conditions. X-ray diffraction data for both compounds were collected using a Rigaku FR-X Ultrahigh Brilliance Microfocus RA generator/confocal optics (Rigaku, Akishima, Japan) with XtaLAB P200 diffractometer [Mo Kα radiation (λ = 0.71075 Å)]. Data for **1** were collected at 173 K, and **2** at 93 K. Intensity data were collected using ω steps accumulating area detector images spanning at least a hemisphere of reciprocal space. Data for all compounds analysed were collected and processed (including correction for Lorentz, polarization, and absorption) using CrystalClear [11]. Structures were solved by Patterson methods (DIRDIF99 PATTY [12]) and refined by full-matrix least-squares against F^2 (SHELXL-2018/3) [13]. Non-hydrogen atoms were refined anisotropically, and hydrogen atoms were refined using a riding model. All calculations were performed using the CrystalStructure interface [14]. Images of structures were generated using OLEX-2 [15]. Selected crystallographic data are presented in Table S1.

4. Conclusions

The title compound (**2**) was synthesized through chlorination of the precursor **1**, which can be easily prepared via lithium–halogen exchange of **P**. Both **1** and **2** have been fully characterized by multinuclear NMR spectroscopy, HRMS, and single-crystal X-ray diffraction. There are very subtle changes in the structural features of **1** and **2** when compared to the phenyl and mesityl equivalents ($\mathbf{B_{Ph}}$, $\mathbf{B_{Mes}}$, and **E**), indicating that although the Lewis acidity of the antimony acceptor group does have an effect, the steric effects introduced in $\mathbf{B_{Mes}}$ may also play a role.

Supplementary Materials: Figure S1: View of H···π interaction in **1**; Figures S2–S11: NMR spectra of **1** and **2**; Figures S12–S15: HRMS of **1** and **2**; Table S1: Selected crystallographic data.

Author Contributions: J.U.B. and B.A.C. carried out the required synthetic steps and preliminary analysis. A.M.Z.S. collected the X-ray data and solved the structures. B.A.C., J.U.B. and P.K. collected and carried out the analysis of the other spectroscopic data. B.A.C. designed the study, analyzed the data, and wrote the manuscript. All authors have read and agreed to the published version of the manuscript.

Funding: This research received no external funding.

Institutional Review Board Statement: Not applicable.

Informed Consent Statement: Not applicable.

Data Availability Statement: CCDC 2260154-2260155 contains the supplementary crystallographic data for this paper. These data can be obtained free of charge from The Cambridge Crystallographic Data Centre via www.ccdc.cam.ac.uk/structures.

Acknowledgments: The authors express gratitude to the University of St. Andrews School of Chemistry and P.K. for use of their laboratory facilities and provision of materials.

Conflicts of Interest: The authors declare no conflict of interest.

References

1. Chalmers, B.A.; Bühl, M.; Athukorala Arachchige, K.S.; Slawin, A.M.Z.; Kilian, P. Structural, Spectroscopic and Computational Examination of the Dative Interaction in Constrained Phosphine−Stibines and Phosphine−Stiboranes. *Chem. Eur. J.* **2015**, *21*, 7520–7531. [CrossRef] [PubMed]
2. Hupf, E.; Lork, E.; Mebs, S.; Chęcińska, L.; Beckmann, J. Probing Donor-Acceptor Interactions in *peri*-Substituted Diphenylphosphinoacenapthyl-Element Dichlorides of Group 13 and 15 Elements. *Organometallics* **2014**, *33*, 7247–7259. [CrossRef]
3. Furan, S.; Hupf, E.; Boidol, J.; Brünig, J.; Lork, E.; Mebs, S.; Beckmann, J. Transition metal complexes of antimony centred ligands based upon acenaphthyl scaffolds. Coordination non-innocent or not? *Dalton Trans.* **2019**, *48*, 4504–4513. [CrossRef] [PubMed]
4. Brünig, J.; Hupf, E.; Lork, E.; Mebs, S.; Beckmann, J. A tetranuclear arylstibonic aicd with an adamantane type structure. *Dalton Trans.* **2015**, *44*, 7105–7108. [CrossRef] [PubMed]
5. Haaland, A. Covalent versus Dative Bonds to Main Group Metals, a Useful Distinction. *Angew. Chem. Int. Ed. Engl.* **1989**, *28*, 992–1007. [CrossRef]
6. Thomas, I.R.; Bruno, I.J.; Cole, J.C.; Macrae, C.F.; Pidcock, E.; Wood, P.A. WedCSD: The online portal of the Cambridge Structural Database. *J. Appl. Cryst.* **2010**, *43*, 362–366. [CrossRef]
7. Batsanov, S.S. Van der Waals Radii of Elements. *Inorg. Mater.* **2001**, *37*, 871–885. [CrossRef]
8. Herrmann, W.A.; Karsch, H.H. *Synthetic Methods of Organometallic and Inorganic Chemistry Volume 3: Phosphorus, Arsenic, Antimony and Bismuth*; Thieme: New York, NY, USA, 1996; pp. 210–213.
9. Wawrzyniak, P.; Fuller, A.L.; Slawin, A.M.Z.; Kilian, P. Intramolecular Phosphine-Phosphine Donor-Acceptor Complexes. *Inorg. Chem.* **2009**, *48*, 2500–2506. [CrossRef]
10. Chalmers, B.A.; Athukorala Arachchige, K.S.; Prentis, J.K.D.; Knight, F.R.; Kilian, P.; Slawin, A.M.Z.; Woollins, J.D. Sterically Encumbered Tin and Phosphorus *peri*-Substituted Acenaphthenes. *Inorg. Chem.* **2014**, *53*, 8795–8808. [CrossRef] [PubMed]
11. *CrystalClear-SM Expert v2.1*; Rigaku Americas: The Woodlands, TX, USA; Rigaku Corporation: Tokyo, Japan, 2015.
12. Beurskens, P.T.; Beurskens, G.; de Gelder, R.; Garcia-Granda, S.; Gould, R.O.; Israel, R.; Smits, J.M.M. *DIRDIF-99*; Crystallography Laboratory, University of Nijmegen: Nijmegen, The Netherlands, 1999.
13. Sheldrick, G.M. Crystal structure refinement with SHELXL. *Acta Crystallogr. Sect. C Struct. Chem.* **2015**, *71*, 3–8. [CrossRef] [PubMed]
14. *CrystalStructure v4.3.0*; Rigaku Americas: The Woodlands, TX, USA; Rigaku Corporation: Tokyo, Japan, 2018.
15. Dolomanov, O.V.; Bourhis, L.J.; Gildea, R.J.; Howard, J.A.K.; Puschmann, H. OLEX2: A complete structure solution, refinement and analysis program. *J. Appl. Cryst.* **2009**, *42*, 339–341. [CrossRef]